The Effects of Polymer-Nanofiller Interactions on the Dynamical Mechanical Properties of PMMA/$CaCO_3$ Composites Prepared by Microemulsion Template

Xi Qiang,[1] Zhao Chunfang,[1] Yuan JianZun,[2] Cheng Shi Yuan[2]

[1]*Department of Pharmacy, WuHan Institute of Chemical Technology, WuHan, 430074, China*
[2]*College of Chemistry & Material Science, HuBei University, WuHan, 430063, China*

Received 28 December 2002; accepted 20 August 2003

ABSTRACT: We prepared novel poly(methyl methacrylate) (PMMA)/$CaCO_3$ nanocomposites by using reverse micelle as a template. The nanoparticles of $CaCO_3$ were prepared by the reverse microemulsion with functional monomer, methyl methacrylate (MMA) as oily phase, and the PMMA/$CaCO_3$ nanocomposite was obtained via polymerization of MMA monomer. The SEM image showed that the nanoparticles of $CaCO_3$ were dispersed in the polymer matrix. Dynamic mechanical analysis (DMTA) was performed to investigate the interaction between the nanoparticles and the polymer chains. In the low-temperature ripening process, two tan δ peaks were observed in the nanocomposite, corresponding to the glass transitions of the matrix and the interface layer. In the high-temperature ripening process, only one tan δ peak was observed, suggesting that the interface layer forms a continuous phase. The nanoparticles behave as a physical crosslinker in the interface layer. Modification of the surface of nanoparticles with polyacrylamide and poly(*N*,*N*′-methylenedisacrylamide) in the nanocomposite did not show an appreciable effect on the interaction of nanoparticles with the matrix. Upon removal of the aqueous phase around the nanoparticles, we obtained surface-capped nanoparticles by using an improved reverse microemulsion technique. Another PMMA/$CaCO_3$ nanocomposite was also obtained with these modified nanoparticles. DMTA analysis of this nanocomposite demonstrated that the aqueous phase layer around the nanoparticles does not significantly affect the interaction between the nanoparticles and the polymer chains. © 2004 Wiley Periodicals, Inc. J Appl Polym Sci 91: 2739–2749, 2004

Key words: reverse microemulsion; PMMA; nanocomposites; mechanical properties; phase separation

INTRODUCTION

Polymer/inorganic nanoparticle nanocomposites have been the focus of extensive research efforts in past decades.[1–4] The introduction of inorganic nanoparticles into a polymer matrix has proved to be an effective method to improve the performance of polymer materials.[5–6] Some unexpected properties of the materials, such as superconductivity,[7] magnetism,[8] nonlinear optics,[9] thermal stability,[10] and dynamic mechanical properties, have been observed because of the enormous interfacial adhesion area of the nanoparticles.[11,12] As a consequence, the nanocomposite properties are strongly influenced by the nature of the interface between inorganic and polymer matrices. A strong interfacial interaction between the inorganic nanoparticles and the polymer matrix can give rise to some unusual properties in these materials.[13]

Several methods have been used to produce polymer nanocomposites, such as sol-gel reaction,[14] intercalative polymerization,[15] polymerization,[16] via melt-processing, depending on the nature of nanoparticles and on the synthetic process of the polymeric matrices. Conventionally, polymerization of monomers and formation of inorganic nanoparticles are separately performed, and the polymer and nanoparticles are mechanically mixed to form nanocomposites.[17] However, it is extremely difficult to disperse the nanoparticles homogeneously into the polymer matrix because of the easy agglomeration of nanoparticles and the high viscosity of the polymer. In recent years, much attention has been paid to the *in situ* synthesis of nanocomposites. This preparation strategy is carried out via polymerization of the polymeric matrices in the presence of the nanofillers.[18] Prior to the dispersion, the inorganic nanoparticles must be modified with organic materials to improve their compatibility and dispersion. Many organic substances have been used to modify the inorganic nanoparticles, such as organic acid,[6] surfactant,[19] and block copolymer.[20] Nevertheless, nanoparticle agglomeration in the modification process with organic substances has remained a major problem because of the enormous interfacial areas of nanoparticles. Therefore, the dispersion of inorganic nanoparticles in the precursors

Correspondence to: X. Qiang (xiqiang64@163.com).

Journal of Applied Polymer Science, Vol. 91, 2739–2749 (2004)

still presents one of the key challenges for *in situ* polymerization.

Water in oil (w/o) microemulsions generally consist of small water droplets surrounded by a surfactant monolayer and dispersed in an oil-rich continuous phase.[21] The particle size of water droplets is under 100 nm, allowing the controlled synthesis of inorganic nanoparticles. Hence, the water droplet is also called a microreactor[22] and has been used for the chemical preparation of relatively monodispersed nanoparticles of various inorganic materials.[23–24] The main goal of this research was to take advantage of the good dispersion of such microreactors in an oily phase to synthesize the nanoparticles of calcium carbonate ($CaCO_3$) with methyl methacrylate (MMA) as the oil phase rather than as a nonreactive solvent and to polymerize MMA in the presence of nano-$CaCO_3$ as nanofillers. The advantage of this methodology for preparation of polymer/nano-inorganic hybrids is to simplify the process of modifying inorganic nanoparticles with organic materials and to disperse these nanoparticles into the precursors. The properties of poly(methyl methacrylate) (PMMA)/$CaCO_3$ nanocomposites were characterized by TEM, SEM, and dynamic mechanical thermal analysis (DMTA). Our DMTA analysis confirmed the existence of the interaction between the nano-calcium carbonate and the polymer chains and of the interfacial layer between the nanofiller and the matrix. It was found that the aqueous phase around the nanoparticles did not significantly affect the interaction of nano-calcium carbonate with polymer chains.

EXPERIMENTAL

Materials

Sodium di(2-ethylhexyl) sulfosuccinate (AOT; 99%, Tokyo Kasei Kogyo Co., Ltd.) and MMA (99%, Aldrich) were used as received. Methanol, CH_3OH, sodium carbonate, Na_2CO_3, and calcium chloride, $CaCl_2$, were of pure grade from Shanghai Reagent Corp. (Shanghai, China). Distilled water was used to prepare all water solutions. All reagents were used without further purification.

Synthesis of nano-$CaCO_3$ particles

Nanoparticles of $CaCO_3$ were prepared in an inverse microemulsion containing the three following common components: 0.575 g AOT surfactants, 0.2 g of 0.247*M* Na_2CO_3 aqueous solution, and 5 g MMA labeled as E1; and 0.575 g AOT surfactants, 0.2 g of 0.25*M* $CaCl_2$ aqueous solution, and 5 g MMA labeled as E2. Nano-$CaCO_3$ reverse microemulsion was formed by mixing E1 and E2 with vigorous stirring. Upon adding 10 mL methanol to the nano-$CaCO_3$ reverse microemulsion, a white floccular material was produced. The $CaCO_3$ nanoparticles were obtained by centrifugation, further washed with methanol three times, and finally dried at 50°C.

Synthesis of PMMA/$CaCO_3$ nanocomposites

To prepare the PMMA/$CaCO_3$ nanocomposite, we used the following procedure. First, we labeled 0.575 g AOT surfactants, 0.2 of 0.247*M* Na_2CO_3 aqueous solution, and 5 g MMA as E1 and 0.575 g AOT surfactants, 0.2 g 0.25*M* $CaCl_2$ aqueous solution, and 5 g MMA as E2, respectively. The nano-$CaCO_3$ reverse microemulsion was subsequently formed by mixing E1 and E2 with vigorous stirring. The system was deaerated with pure nitrogen at 20°C and then the temperature was raised to 50°C. Subsequently, radical polymerization was initiated upon the addition of 0.001 g AIBN while stirring. At a much higher MMA viscosity, the liquid was poured into the module and the temperature was raised to 80°C (a low-temperature ripening process) or 100°C (a high-temperature ripening process) for ripening for 1 week and 2 days under nitrogen atmosphere, respectively. Reverse microemulsion/PMMA composites were prepared with the same weight of 0.25*M* NaCl aqueous solution instead of 0.25*M* $CaCO_3$ aqueous solution with other components remaining unchanged. Other procedures were the same as above.

Analysis

Transmission electron microscopy. Electron micrographs were recorded with an electron microscope (Model JEM-100CXII). Samples for electron microscopy were prepared by placing a drop of nano-$CaCO_3$ reverse microemulsion onto a copper grid coated with a thin carbon film and keeping the evaporation of the solvent at room temperature.

Scanning electron microscope. To examine the degree of nanoparticle dispersion in the polymer matrix, the nanocomposites were broken into fragments and the fractured surfaces were observed by using a scanning electronic microscope. This analysis was carried out with a Philips SEM JSM-5510LV electron microscope, and the scanning electron micrographs were taken on Au-coated surfaces of the specimens.

Dynamic mechanical analysis. Rheometric Scientific MK^{III} apparatus was used to follow dynamic mechanical behavior of hybrids by 2°C/min and 5 Hz at 25–200°C.

RESULTS

Morphology of $CaCO_3$ nanoparticles and nanocomposite

The nano-$CaCO_3$ was prepared by mixing the $CaCl_2$ reverse microemulsion and the Na_2CO_3 reverse micro-

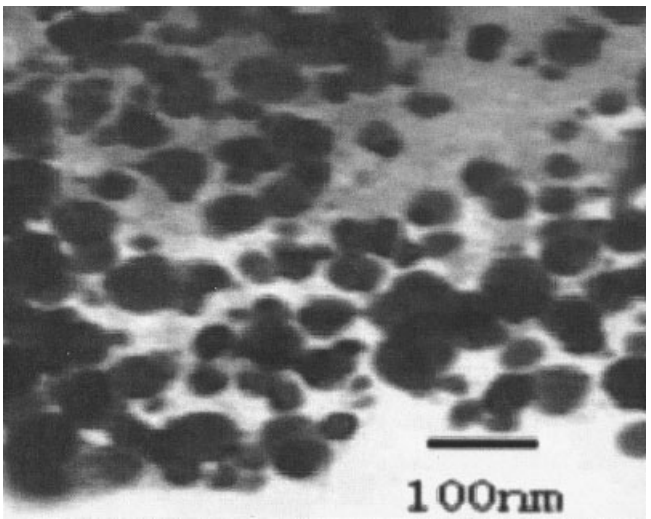

Figure 1 TEM photograph of nano-$CaCO_3$.

emulsion together as described in Experimental. The morphology of nano-$CaCO_3$ was characterized with TEM; the range of particle size was 20–80 nm, as shown in Figure 1.

Upon the reverse microemulsion polymerization, the PMMA/$CaCO_3$ nanocomposite was analyzed with SEM and the image is shown in Figure 2. It is seen that the $CaCO_3$ sphere particles are well dispersed in the PMMA matrix. The observed particles are the reverse micelles of the $CaCO_3$ nanoparticles. The particle size is clearly bigger than that shown in Figure 1 for two reasons. First, the particle size depends on the water content in the reverse micelles. The TEM spectroscopy was conducted at high vacuum. The $CaCO_3$ nanoparticles were in the reverse micelles prior to the MMA reverse microemulsion; the water content was removed via the vacuum. As a consequence, the only $CaCO_3$ nanoparticles coated with a monosurfactant layer were observed as depicted in Figure 1. However, upon polymerization with MMA, which serves as the continuous phase, the reverse micelles were well dispersed in PMMA. The core of these micelles is the $CaCO_3$ nanoparticle surrounded by the NaCl aqueous solution and the surfactant layer and thus the size of the nanoparticles becomes much bigger (Fig. 2). Second, the interface energy of the solvent/aqueous phase is now replaced with that of the polymer/aqueous phase after polymerization of MMA, resulting in an increased particle size.[25]

Dynamic mechanical properties and interface

Valuable information on morphology and mainly on the interface of polymer matrix and the fillers in the composite can be obtained from DMTA.

Function of nanofiller and interface structure

Figure 3 shows the tensile storage modulus $E'(T)$ and the loss factor tan δ as a function of temperature for the systems we studied. The change in the storage modulus of the hybrid networks [Fig. 3(a)] is accompanied by the change in the loss factor tan δ [Fig. 3(b)]. The peak of tan δ, located at about 135.58°C, is the glass transition temperature (T_g) of the neat PMMA network [curve 1, Fig. 3(b)]. The height of the tan δ peak located at 55°C in curve 2 [Fig. 3(b)], which corresponds to the glass transition of the reverse-micelle/PMMA network, is lower than that of the tan δ peak for PMMA at about 135.58°C and increases slowly initially and then sharply away from 55°C. Higher content of surfactant is one of the basic characteristics in the reverse micelle. The sphere reverse micelles serve as a plasticizer, which reduces the crosslink density of PMMA and the volume fraction of the free nonhindered chains of the organic network. This results in smaller storage modulus E' and tan δ as well as in lower T_g. From curves 2 and 3, the great change in the storage modulus and tan δ is obvious. The peak of tan δ at 110°C, which corresponds to the glass transition of the nano-$CaCO_3$/PMMA nanocomposite, increases and a new damping peak of tan δ appears at a higher temperature, which provides evidence on the phase separation in the nanocomposite.[26] The new peak located above 145.64°C can be attributed to the glass transition of the organic network chains with reduced mobility due to their interaction with nano-$CaCO_3$. The region of the polymer chains with reduced mobility as an interface layer is located around the nanoparticles $CaCO_3$. For the part of surfactants dissolved in the network PMMA, the glass transition temperature of the matrix (110°C) is lower than that of PMMA (135.58°C).

Comparing curve 3 with curve 3′ in Figure 3, one observes only one peak of tan δ located at the

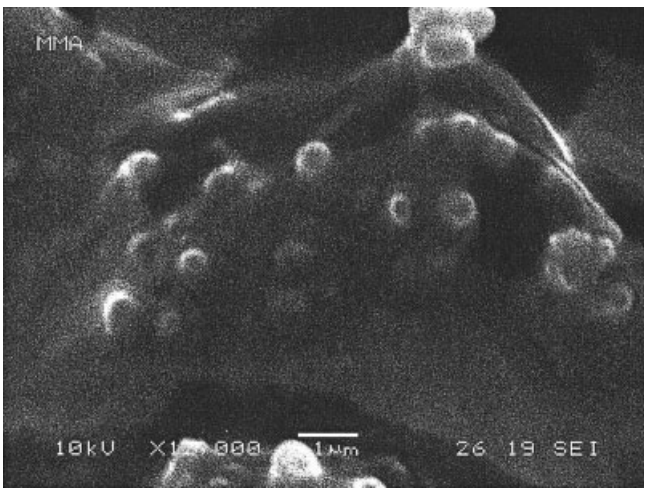

Figure 2 SEM photograph of nano-$CaCO_3$/PMMA.

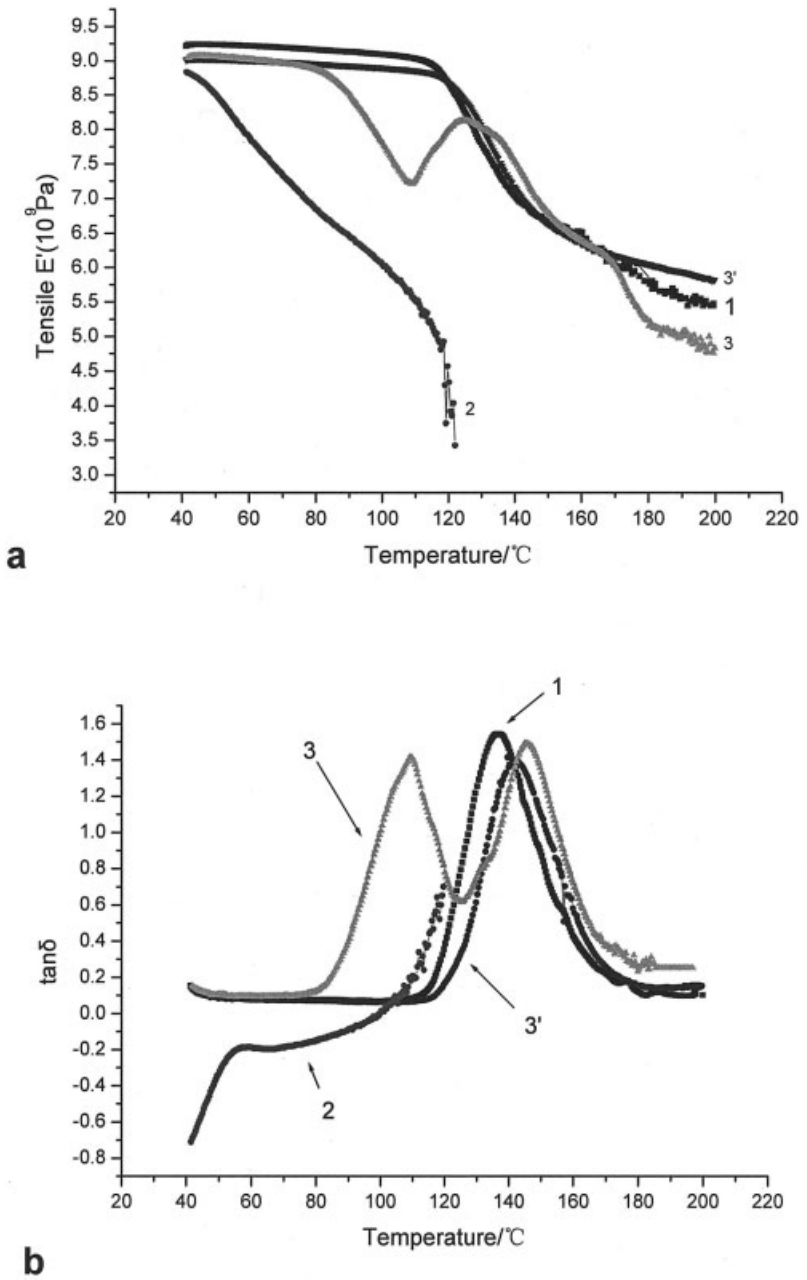

Figure 3 The dynamic tensile storage modulus E' (a) and loss factor tan δ (b) of the PMMA and nanocomposite as a function of temperature. 1: PMMA; 2: reverse-micelle/PMMA; 3: nano-$CaCO_3$/PMMA [0.5*M* $CaCO_3$ (wt 0.1536%) in the low temperature ripening process]; 3′: nano-$CaCO_3$/PMMA [0.5*M* $CaCO_3$ (wt 0.1536%) in the high-temperature ripening process].

141.78°C, which corresponds to the glass transition of nano-$CaCO_3$/PMMA. No phase separation phenomenon was observed. The difference of the two composites is only the temperature of the ripening process. Curve 3′ represents the high-temperature ripening process. Higher temperature enhances the interaction between the nanoparticles and the polymer chains. A strong interaction gives rise to a large interface layer and facilitates the formation of a continuous phase.

From Figure 3(a), curve 3′ approximately forms a plateau at around 150°C and another plateau in the range from 150 to 170°C. The plateau modulus above T_g results from the crosslinking between the polymer matrix and the nanofiller.[27]

Interface layer structure

To investigate the effect of the interface structure on the glass transition and the dynamic mechanical properties, we synthesized polyacrylamide and poly(*N*,*N*′-methylenedisacrylamide) around the nanoparticles in the interface layer by using the following procedure.

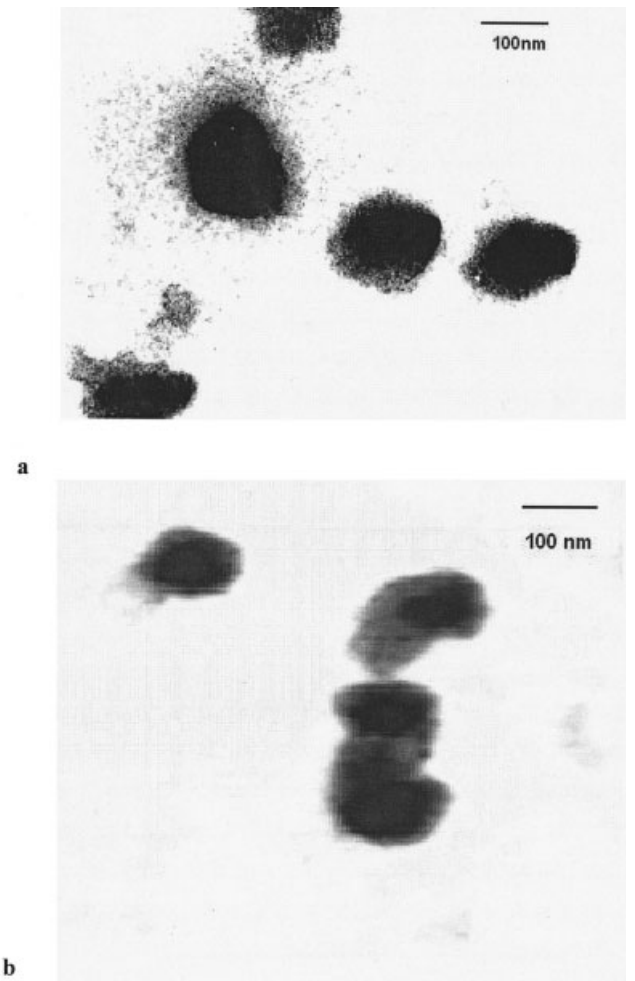

Figure 4 TEM photograph of the nano-$CaCO_3$ modification with polyacrylamide (a) and poly(*N*,*N*′-methylenedisacrylamide) (b).

First, the nano-$CaCO_3$ inverse microemulsion of MMA as the oily phase was prepared by using 1.2 g AOT surfactants, 0.4 g 0.30*M* nano-$CaCO_3$, and 10 mL MMA and acrylamide or *N*,*N*′-methylenebisacrylamide, which is 1.5 times the $CaCO_3$ weight. The microemulsion was deaerated with pure nitrogen at 20°C, and then two drops of ammonium persulfate (10 μg/mL) was injected. The core-shell structure of nano-$CaCO_3$/polyacrylamide was prepared at 40°C for 4 h and then we let it cool down for examination in the next step. Its morphology was investigated with TEM and the results are shown in Figure 4. Next, the microemulsion was deaerated with pure nitrogen at 20°C and then the temperature was raised to 50°C. The MMA was polymerized by adding 0.001 g AIBN. The other preparation procedures were the same as those for the nano-$CaCO_3$/PMMA nanocomposite at the high- and low-temperature ripening processes described in Experimental.

The photograph in Figure 4 shows that core-shell structure morphology exists in the composite as expected. Shell layer of polyacrylamide around the particles can be observed. The same morphology of the shell layer of poly(*N*,*N*′-methylenedisacrylamide) was also obtained. After polymerization of MMA, the nanocomposite was prepared and its dynamic mechanical analysis is presented in Figure 5. The dynamic mechanical curve is the same regardless of the temperature ripening process.

As discussed above, there is an interface layer in the nano-$CaCO_3$/PMMA composite. We modified this interface layer with acrylamide or *N*,*N*′-methylenebisacrylamide. This thin layer is inside the interface layer around the particle. George et al.[28] reported that there was a tight layer in the filled polymers: polymer chains in this layer were immobile and generally the thickness of the tight bound varied between 0.5 and 2 nm. It is well known that microphase separation is detectable by DMTA only if the domains exceed a critical size of about 5–10 nm and, in general, this tight layer in the composite is not thick enough to be detected by the dynamic mechanical measurements. The mobility of the polymer chains is rather restricted, which in return limits the mobility of the rest of the interface layers, normally known as the loose layer, because the tight layers also affect the polymer chain configuration. The loose layer and the tight layer constitute the intermediate layer, which can be readily probed by DMTA if it exceeds a certain thickness. Hence, there are three phases in the composite as follows: the matrix, the interface layer, and the filler. The interface layer is composed of a loose layer and a tight layer. The properties of the tight layer are dictated by the interaction between the polymer chains and the nanoparticles, while the loose layer is controlled by the tight layer. Many studies[29–30] have found two prominent features in the tan δ versus temperature spectrum in the fine inorganic particles filled in the polymer systems. One corresponds to the glass transition of the polymer matrix and another reflects the glass transition of the interface layer where the polymer chains are restricted to the loose layer and the tight layer. The polymer chains in the tightly bound layer does not participate in either of the two glass transitions. Analyzing the curves 1, 2, 3, and 4 in Figure 5, one observes only one glass transition in the composite whose corresponding temperature is higher than that of the glass transition of the pure PMMA. This indicates that the loose bound layer is large enough to form a continuous phase and to exhibit its own glass transition. Polyacrylamide and poly(*N*,*N*′-methylenebisacrylamide) polymerize with MMA and form this interface layer. The temperature of glass transition of the curve 2 is 141.64°C, whereas the ones for the curves 3 and 4 are 140.2 and 142.18°C, respectively. The differences among glass transition temperatures of the curves 2, 3, and 4 are marginal, indicating that the properties of the polymer chains in

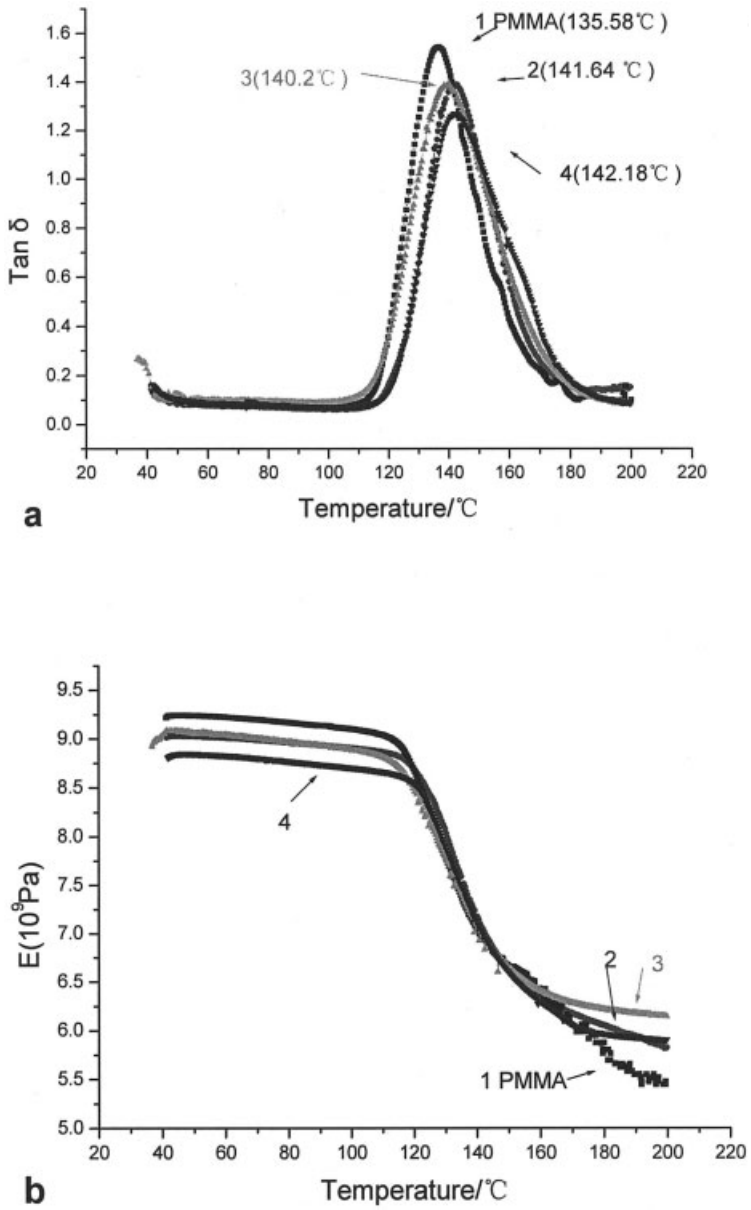

Figure 5 Comparison of the tensile storage E' and tan δ for various interface layer modifications with 1: PMMA; 2: none; 3: acrylamide; 4: *N*,*N*′-methylenedisacrylamide in the nano-$CaCO_3$/PMMA nanocomposite.

the intermediate layer among these complexes, and thus the properties of the tight layer and the loose layer at the interface, are rather similar. Therefore, the adsorptive interaction between the polymers and the nanoparticles in these complexes are very similar. The above results further suggest that the surface modification on the $CaCO_3$ nanoparticles with the polymer (polyacrylamide) and the crosslinker [poly-(*N*,*N*′-methylenebisacrylamide)] has little effect on the polymer chains absorbed on the surface of the nanoparticles and that the aqueous phase layer around the nanoparticles does not significantly affect the interaction between the polymer chains and the nanoparticles. The polymer chains absorbed on the surface of the inorganic and organic particles do not radically change the ability of the particle adsorption, which may be determined by the particle size and the ripening temperature. To further investigate the effect of the aqueous phase around the nanoparticles in the nanocomposites on the interaction between the polymer chains and the nanoparticles, we modified the nanoparticles of $CaCO_3$ by an improved inverse microemulsion technique as follows: We first labeled 0.575 g AOT surfactants, 0.3 g butanol, 0.2 g 0.247*M* Na_2CO_3 aqueous solution, and 5 g heptane as E1 and 0.575 g AOT surfactants, 0.3 g butanol, 0.2 g 0.26*M* $CaCl_2$ aqueous solution, and 5 g heptane as E2. The nano-$CaCO_3$ reverse microemulsion was formed by

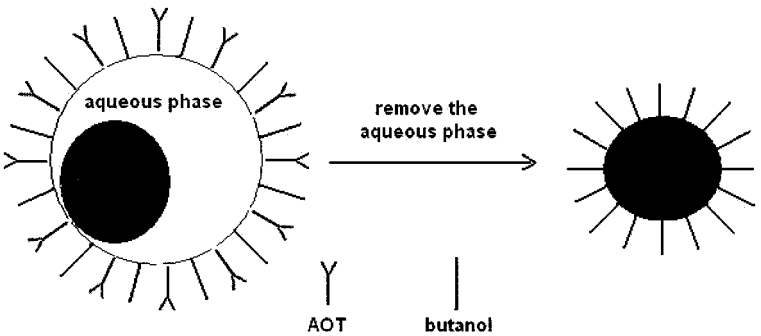

Figure 6 Schematic illustration of the formation of strong surface-modified nanoparticles of $CaCO_3$.

mixing E1 and E2 with vigorous stirring. Upon raising the temperature for 2 h and then cooling the system down to room temperature, followed by adding 30 mL methanol, we obtained a white precipitate by centrifugation. We washed the material with methanol and centrifuged it again. Another white precipitate was obtained. Repeating this procedure three times, we added 10 mL MMA to this material and then dispersed the complex using supersonics for 30 min. The material was polymerized by adding 0.01 g AIBN induction agent. The polymerization procedure is similar to the one described in Experimental.

Aqueous phase in the interface layer

In the above experiment, the surface capping reagent butanol served as a cosurfactant in the inverse microemulsion and was used simultaneously with the surfactant AOT to prepare the surface-modified nanoparticles of $CaCO_3$. This is an effective way[31] to modify the surface of nanoparticles because the cosurfactant is chemisorbed uniformly on the surface of particles. The molar ratio of Ca^{2+} to CO_3^{2-} is larger than 1, allowing a sufficient amount of Ca^{2+} ions on the surface of the nanoparticles to react with butanol. The role of the reflux is mainly to remove water from the micelles and to enhance the effectiveness of the modification of the nanoparticles, as illustrated in Figure 6.

Figure 7 displays the dynamic properties of PMMA/$CaCO_3$ nanocomposite and PMMA/$CaCO_3$ (butanol modified) nanocomposite. There is no aqueous phase in the interface layer in the PMMA/$CaCO_3$ (butanol modified) nanocomposite but there is aqueous phase in the PMMA/$CaCO_3$ nanocomposite. We observed little difference in the dynamical mechanical curves between the high- and the low-temperature ripening processes. Indeed, comparing the temperature-dependent loss factor profiles described by curve 1 and curve 2, one sees similar behavior with marginal difference in magnitude. The T_g of the nanocomposite of the nonaqueous phase layer is 142.8°C, which is slightly higher than that of the aqueous phase layer (141.64°C). Furthermore, the modulus of curve 1 is higher than that of curve 2 before and after the glass transition. For surfaces capped with the nanoparticles, there are nonsurfactants in the composite, which makes the volume fraction of PMMA in the composite higher. Consequently, the modulus of PMMA/$CaCO_3$ (butanol modified) nanocomposite becomes higher than that of the PMMA/$CaCO_3$ nanocomposite.

Comparing curve 1 with curve 2, we conclude that the aqueous phase layer around the nanoparticles does not significantly affect the interaction between the nanoparticles and the polymer chains in the interface layer. However, the modulus of the nanocomposites is considerably affected by the surfactants in the composites.

Effect of particle size on the interface

Low temperature ripening process. Figure 8 shows the profiles of tan δ (a) and the storage module (b) versus temperature at various concentrations of $CaCO_3$ in the composite in the low-temperature ripening process. Two peaks in the tan δ profile, corresponding to the interface layer and the matrix, are observed for the composite of 0.5*M* nano-$CaCO_3$. For the composite of 0.1*M* nano-$CaCO_3$, the main feature corresponds to the interface layer, while the shoulder reflects matrix. Figure 8 illustrates that the volume fraction of the interface layer of the 0.1*M* nano-$CaCO_3$ composite is larger than that of the 0.5*M* nano-$CaCO_3$ composite. In the reverse microemulsion system, with the same surfactant weight in the aqueous phase, the particle size decreases as the concentration of $CaCO_3$ decreases. Thus, the particle size of the 0.1*M* nano-$CaCO_3$ composite is smaller than that of the 0.5*M* nano-$CaCO_3$ composite. In the low-temperature ripening process, as the particle size decreases (by reducing the concentration or the weight percentage of $CaCO_3$), the volume fraction of the interface layer increases. This indicates that a stronger interaction between the polymer chains and the small $CaCO_3$ nanoparticles leads to a larger volume fraction of the interface. Figure 8(b)

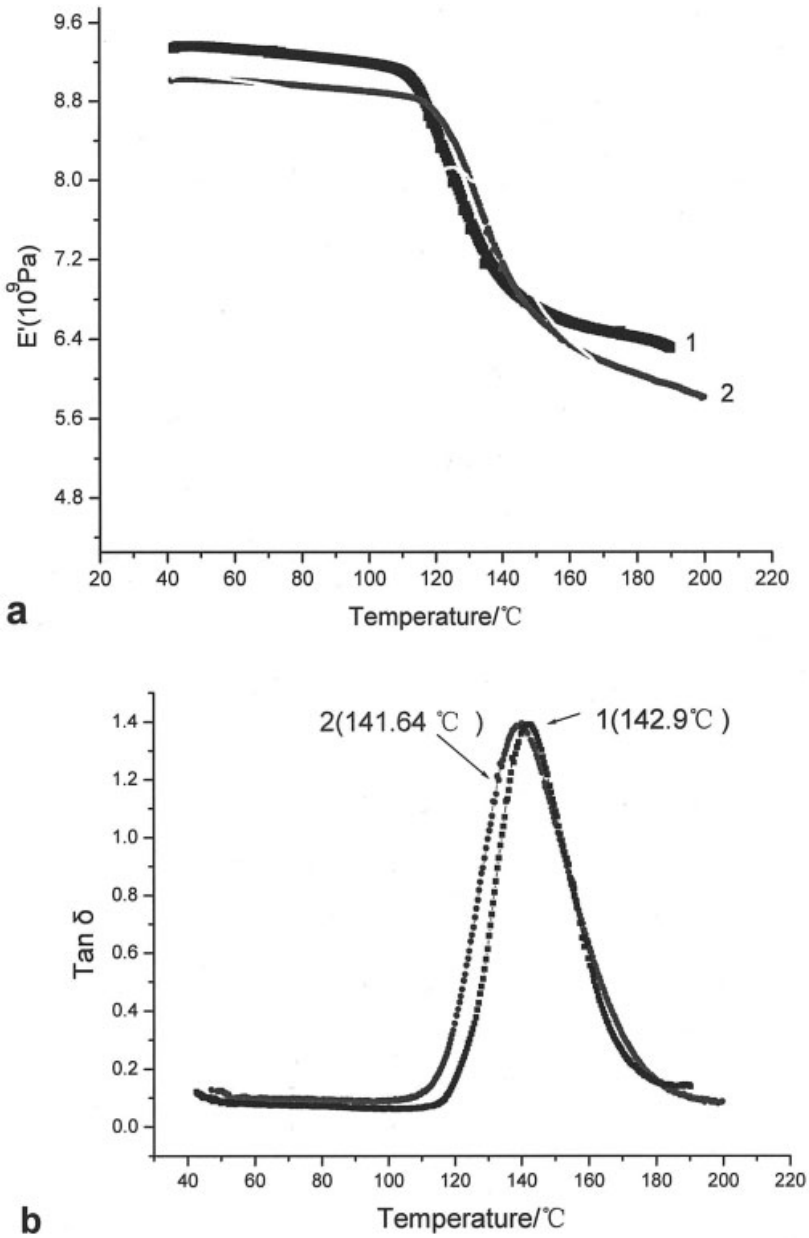

Figure 7 Comparison of the tensile storage modulus (E') (a) and the loss factor tan δ (b) of the nanocomposite of 1: the nonaqueous phase in the interface layer; 2: the existing aqueous phase in the interface layer. The weight content of $CaCO_3$ in both specimens is 0.0921%.

displays the modulus versus the temperature. A peak at about 130°C and a small plateau are observed from 143 to 170°C, and the modulus decreases sharply as the temperature exceeds 170°C for 0.5*M* $CaCO_3$. For 0.1*M* $CaCO_3$, however, a small plateau from 130–140°C is observed and the modulus decreases slowly. This suggests that the smaller the particle size of the $CaCO_3$ nanoparticles, the large the modulus is. Therefore, a smaller particle size gives rise to a stronger interaction between the matrix and the nanoparticles and a larger volume fraction of the interface layer.

High temperature ripening process. Figure 9(a) displays the T_g of the nanocomposites versus the concentration of $CaCO_3$. Our results indicate that the T_g increases as the concentration of $CaCO_3$ decreases. As discussed above, the particle size of the nanoparticles decreases as the concentration of $CaCO_3$ decreases. In the high-temperature ripening process, with a smaller particle size of the nanoparticles, the glass transition temperature becomes higher. These results indicate that the interaction between the matrix and the nanoparticles becomes stronger, while the size of the nanoparticles becomes smaller. This is consistent with the results obtained for the lower temperature process.

In the high-temperature ripening process, Figure 9(b) shows the tensile storage modulus versus temper-

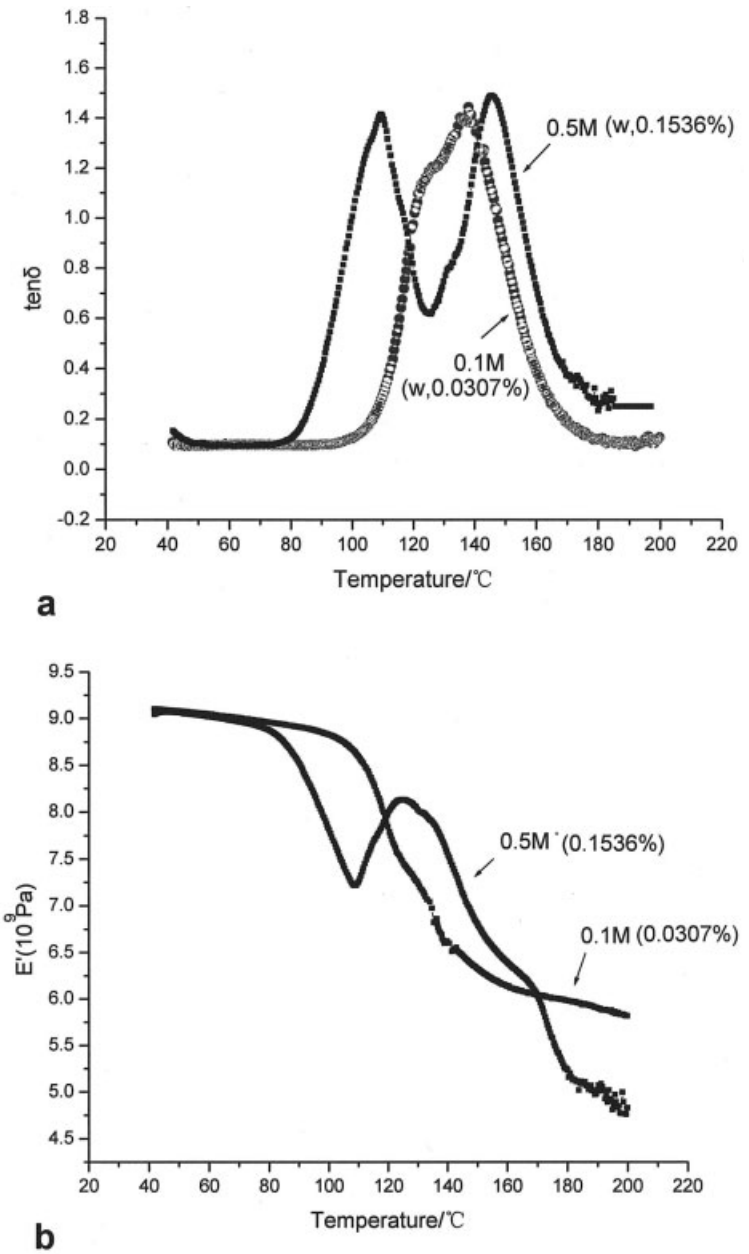

Figure 8 The effect of the particle size on the dynamic mechanic properties in the low-temperature ripening process. (a) tan δ versus temperature with various concentrations of $CaCO_3$. (b) The tensile storage modulus (E') versus temperature with various concentrations of $CaCO_3$.

ature at various concentrations of the nano-$CaCO_3$ (via weight fraction). Clearly, the modulus increases slightly as the concentration of the nanoparticles decreases. As discussed above, the smaller the concentration of the nanoparticles, the smaller the particle size becomes. This suggests that the particle size does not significantly affect the modules of the nanocomposites in the higher ripening process.

CONCLUSIONS

In summary, we prepared the nanoparticles of $CaCO_3$ by the reverse microemulsion with a functional monomer, MMA, as the oily phase. The TEM photograph shows that the particle size is under 20–80 nm. The SEM photographs indicate that the nanoparticles of $CaCO_3$ are dispersed in the polymer matrix. The dynamic mechanical analysis demonstrates that the interface layer is formed around the nanoparticles. The polymer chains in the interface layer are restricted because of the strong interaction among the nanoparticles. The glass transition temperature of the interface layer is higher than that of the matrix because the mobility of the polymer chains is restricted for the interaction of polymer with nano-$CaCO_3$ and the nanoparticles may behave as the crosslinker in the interface layer.

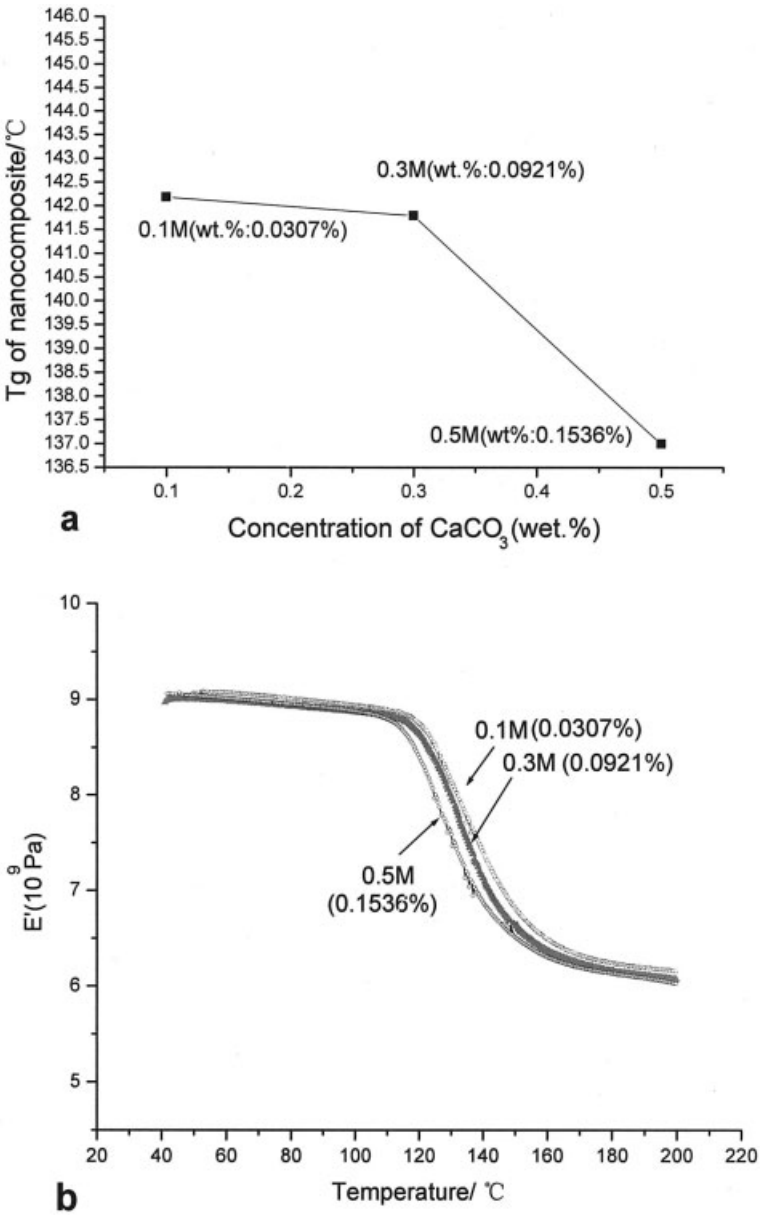

Figure 9 The effect of the particle size on the dynamic mechanic properties in high-temperature ripening process. (a) The concentration effect of $CaCO_3$ on T_g. (b) The tensile storage modulus (E') versus temperature with various concentrations of $CaCO_3$.

We found that the ripening process affects the interaction between the nanoparticles and the polymer chains considerably. In the high-temperature ripening process, the interface layer is overlapped and combined with the matrix to form the continuous phase. Furthermore, we attempted to modify the nanoparticle surface with other polymers, which did not result in a significant change in the dynamic mechanical properties of the nanocomposites. Finally, we prepared the nanocomposite with nano-$CaCO_3$ capped with butanol followed by removing the aqueous phase around the nanoparticles. The DMTA analysis revealed that the aqueous phase layers around the nanoparticles do not significantly affect the interaction between the nanoparticles and the polymer chains in the nanocomposite. It was found that the detailed characteristics of the glass transition and the storage modulus are dependent upon the particle size as well as upon the ripening process.

References

1. Ramos, J.; Millan, A.; Palacio, F. Polymer 2000, 41, 8461.
2. Zhu, Z. K.; Yin, J.; Cao, F.; Shang, X. Y.; Lu, Q. H. Adv Mater 2000, 20, 1055.
3. Chen, T. K.; Tien, Y. I.; Wei, K. H. Polymer 2000, 41, 1345.

4. Mukheerjee, M.; Datta, A.; Chakravorty, D. Appl Phys Lett 1994, 64, 1159.
5. Okamoto, M.; Morita, S.; Taguchi, H.; Kim, Y. H.; Kotaka, S.; Tateyama, H. Polymer 2000, 41, 3887.
6. Avella, M.; Errico, M. E.; Martuscelli, E. Nano Lett 2001, 4, 213.
7. Nagaoka, K.; Naruse, H.; Shinohara, I. J Polym Sci: Polym Lett Ed 1984, 22, 659.
8. Palacio, F.; Maron, M.; Garin, J.; Reyes, J.; Fontcuberta, J. Mol Cryst Liq Cryst Sci Technol 1989, 176, 415.
9. Shiraishi. Y.; Toshima, N. Colloid Surf A 2000, 169, 59.
10. Gotoh, Y.; Igarashi, R.; Ohkoshi, Y.; Nagura, M.; Akamatsu, K.; Deki, S. J Mater Chem 2000, 10, 2548.
11. Sawai, D.; Miyamoto, M.; Kanamoto, T.; Ito, M. J Polym Sci: Polym Phys Ed 2000, 38, 2571.
12. Hong, S. U.; Jin, J. H.; Won, J.; Kang, Y. S. Adv Mater 2000, 12, 968.
13. Hartley, F. R. Chem Rev 1973, 73, 163.
14. Noell, J. L. W.; Wilders, G. L.; McGrath, J. E. J Appl Polym Sci 1990, 40, 1177.
15. LeBaron, P. C.; Wang, Z. J Appl Clay Sci 1999, 15, 11.
16. Vaia, R. A.; Jandt, K. D.; Giannelis, E. P. Macromolecules 1990, 28, 8080.
17. Ghosh, K.; Maiti, S. N. J Appl Polym. Sci 1996, 60, 323.
18. Zhang, Z.; Zhang, L.; Wang, S.; Chen, W.; Lei, Y. Polymer 2001, 42, 8315.
19. Su, S.-J.; Kuramoto, N. Synth Met 2000, 114, 147.
20. Limin, Q.I.; Colfen, H.; Antonietti, M. Nano Lett 2001, 2, 61.
21. Jada, A.; Lang, J.; Zana, R. J Phys Chem 1989, 93, 10.
22. Markus, A.; Beate, S. Macromolecules 1991, 24, 6636.
23. Pileni, M. P. J Phys Chem 1993, 97, 6961.
24. Jada, A.; Lang, J.; Zana, R. J Phys Chem 1989, 93, 10.
25. Fukuoka, A.; Ichikawa, M. J Am Chem Soc 2001, 123, 3373.
26. Mateia, L.; Dukh, O.; Kolarik, J. Polymer 2000, 41, 1449.
27. Landdry, C. J. T.; Coltrain, B. K.; Brady, B. K. Polymer 1992, 33, 1486.
28. Geroge, T.; Eisenberg, A. Macromolecules 1995, 28, 6067.
29. Landry, G. J. T.; Coltrain, B. K. Macromolecules 1993, 26, 3702.
30. Matejka, L.; Kolarik, J. Polymer 2000, 41, 1449.
31. Steigerwald, M. L.; Brus, M. E. J Am Chem Soc 1988, 110, 3046.